Numerical modelling and parametric study of the melting behaviour of ice crystal particles

Xin Yang*, Matthew McGilvray†, and David Gillespie‡
University of Oxford, Oxford OX2 0ES, UK

Ice crystal icing has been identified as a risk to flight safety, due to its reduction of engine performance, potential to cause engine damage and flameout. A critical factor in the sticking efficiency of ice crystals is the melting behaviour of ice crystals. This paper presents an ice melting model integrated with surface blowing and porosity. A parametric study is performed to understand the effects of flow conditions (total pressure, humidity, total temperature, Mach number, and slip velocity) and particle properties (particle size, aspect ratio, and porosity factor) on ice melting behaviour. The model is compared against the melting time of single ice particles in an acoustic levitator. The results show that employing sphericity and porosity could improve prediction performance. Surface blowing from evaporation increases melting time and its effect is larger with a higher gas temperature. Ice melting time increases with pressure at high humidity, while an opposite trend is observed at low humidity. Increasing gas temperature, humidity, slip velocity, aspect ratio, and particle temperature can decrease ice melting time, while increasing Mach number, particle size, and porosity factor can increase ice melting time. While wet bulb temperature can be used to evaluate ice melting potential when only one flow parameter is varied, it appears insufficient alone under scenarios where multiple flow parameters are changing simultaneously.

I. Nomenclature

A_p and $A_{\mathrm{p},\perp}$	=	particle area and projected particle area, m^2
c_p	=	specific heat, $J/(kg.K)$
D_p	=	volume equivalent particle diameter, m
$D_{\mathrm{v,g}}$	=	water vapour diffusivity, m^2/s
E	=	aspect ratio, [-]
e_σ	=	surface energy, J/m^2

*Postdoctoral researcher, Department of Engineering Science, Oxford Thermofluids Institute, AIAA Member; xin.yang@eng.ox.ac.uk (Corresponding author).
†Associate Professor, Department of Engineering Science, Oxford Thermofluids Institute.
‡Associate Professor, Department of Engineering Science, Oxford Thermofluids Institute.

F_{SB}	=	surface blowing factor, [-]
h	=	specific enthalpy, kJ/kg
k_g	=	gas thermal conductivity, $W/(m.K)$
L_f and L_v	=	latent heat of fusion and evaporation, respectively, J/kg
m	=	mass, kg
MRD	=	mean relative difference, [-]
Ma	=	Mach number
$\dot{m}_{evap}$	=	evaporation mass transfer, kg/s
$\dot{m}_{melt}$	=	melting mass transfer, kg/s
$\dot{m}_{sub}$	=	sublimation mass transfer, kg/s
Nu	=	Nusselt number
P	=	pressure, Pa
Pr	=	Prandtl number
Q_{conv}	=	convective heat flux, W
R	=	universal gas constant, 8.314 $J/(mol.K)$
Re_p	=	particle Reynolds number
RH	=	relative humidity, [-]
Sc	=	Schmidt number
Sh	=	Sherwood number
t	=	time, s
T	=	temperature, K
V	=	velocity, m/s
WBT	=	wet bulb temperature, $°C$
γ_v	=	vapour mass fraction, [-]
γ_f	=	specific heat ratio
μ	=	viscosity, $Pa.s$
ρ	=	density, kg/m^3
Φ	=	sphericity, [-]
Ω	=	humidity ratio, [-]

Subscript

g	=	gas phase

i	=	ice
p	=	particle
s	=	static
w	=	water

II. Introduction

With the continued growth in air travel, it is believed that flights are increasingly operated in hazardous icing conditions. Since 1990 there have been over 240 icing related aircraft engine events and 62 of them are categorized as possibly due to ice crystal icing (ICI) [1]. Several icing codes [2–9] have been developed in order to support preliminary design and certification of de-icing systems. Modelling melting behaviour of ice crystals is important for the development of icing codes since melt ratio contributes significantly to the sticking efficiency of ice crystals. Mason [10] developed the first ice melting model, where the melting process was assumed to be a quasi-steady one-dimensional heat transfer problem of a sphere with a phase change. Melting of ice particles starts when the ice particle temperature reaches the melting point and then a water layer is gradually formed at the outer layer of the ice core. Heat conduction through the water layer is assumed to be steady state and the surface temperature of the water layer is allowed to increase above the melting point during the melting process. Mason found that the model adequately predicted the melting time of ice particles with a radius from 500 to 1500 μm. Rasmussen et al. [11] investigated the melting behaviours of ice particles of a radius from 200 to 500 μm in a wind tunnel. It was found that the measured melting time of ice was lower than the prediction using Mason's melting model. Later, Rasmussen et al. [11, 12] found that the disagreement in the melting time between the predictions and measurements was not only due to neglecting the eccentric location of ice core and the internal circulation of water layer, but also due to overlooking the increased external heat transfer related to the non-spherical geometry of ice particles. Rasmussen et al. [12] proposed an improved ice melting model and improved the predictions of melting time by 15% through using a larger heat transfer coefficient. Recently, Wright et al. [2] presented a melting model of ice crystal particles for engine icing conditions, where the melting process was simplified via the lumped-capacity method. The lumped-capacity method requires less computational efforts compared with the detailed heat conduction model. However, the simplification neglects the heat conduction in the ice particle, in contrast to the detailed melting models proposed by Mason [10] and Rasmussen et al. [12]. Hauk et al. [13, 14] used a lumped-capacity based ice melting model to predict ice melting time in an acoustic levitator under multiple flow conditions (relative humidity, flow velocity and air temperature). The mean relative difference between predictions and measurements was approximately 8% for the spherical ice particles. This implies that the lumped-capacity method could be acceptable for predicting ice melting behaviour under the conditions investigated. For non-spherical ice particles, Hauk et al. [14] showed that using the assumption of spherical ice shape leads to the overprediction of melting time

of non-spherical ice particles by approximately 10-20%. This observation is similar to the findings of Rasmussen et al. [11, 12]. The non-spherical geometry of ice particle can increase the external heat transfer to ice particles and reduce melting time. Currie et al. [15] proposed an empirical non-sphericity correction factor in order to improve the prediction of the melting behaviours of ice crystals. The correction factor is not directly related to non-sphericity, but based on the overall melting behaviours. Hence, the correction factor could be useful for modelling melting when ice particle shapes are unknown. However, using the general correction factor, which is not a function of particle shape parameter, could be risk for ice particles with different non-spherical geometries. Villedieu et al. [3] proposed another improved lumped-based ice melting model by using the sphericity related heat and mass transfer model, which was compared against the melting behaviour of single ice particles in an acoustic levitator by Hauk et al. [14]

These ice melting models have made significant progress in modelling icing melting behaviour. In addition, the previous experimental research has found that melt ratio increases with an increase in temperature and humidity [16–18] and with a decrease in particle size [19]. In particular, wet bulb temperature is found to be a significant indicator of the degree of melting [17]. However, little has been published in relation to the parametric study of flow conditions (pressure, Mach number, slip velocity, etc.) and particle geometry related factors (shape factor, porosity, etc.) on melting behaviours. Furthermore, the effect of surface blowing on ice melting behaviour is often ignored in these existing ice melting models. Surface blowing is the evaporation occurred at particle surface, affecting the fluid properties adjacent to the particle surface [20]. This behaviour could reduce the heat and mass transfer and affect particle melting behaviour. It is important to understand how significant the effect on predicting ice melting behaviour is in order to improve the existing ice melting models. Therefore, this study aims (i) to develop an ice melting model integrated with surface blowing and porosity and (ii) to numerically investigate the effects of flow conditions and particle parameters on the melting behaviour of ice crystal particles. The empirical model proposed by Renksizbulut et al. [20] is employed to take into account the effect of surface blowing. In addition, sphericity is considered in the heat and mass transfer using the method proposed by Villedieu et al. [3].

III. Mathematical models

A. Ice melting model

The ice melting model (ice phase change model) is based on the conservation of energy and mass conservation equations. The lumped-based ice melting model is assumed to predict ice melting behaviour. Commonly, it is assumed ice melting consist of three stages according to the state of ice crystals, (i) fully solid ice crystals, (ii) partially melted ice crystals, and (iii) fully melted ice crystals. During the first stage of fully solid ice crystals, the mass transfer is from the sublimation and the heat transfer is from the convection and phase change heat transfer. Particle shape remains unchanged while the particle size changes with particle mass. During the second stage of partially melted ice crystals,

the mass transfer is from the evaporation and the heat transfer is from the convection, evaporation/condensation, and melting heat transfer. Particle temperature is maintained at the melting temperature of ice. In addition, particle sphericity gradually approaches unity with the assumption of the fully melted particles being spherical droplets. During the third stage of fully melted ice crystals, the mass transfer is from the evaporation/condensation and the heat transfer is from the convective and phase change heat transfer. Particle temperature is able to increase again while the particle shape remains spherical. In the improved ice melting model by Villedieu et al. [3], the effect of non-spherical particle shape on the heat and mass transfer rates is considered by using sphericity, which is used to derive the Nusselt number and Sherwood number, as well as the particle surface area. The effect of surface blowing on the melting behaviour of ice particles is taken into account using the model proposed by Renksizbulut et al. [20], which is a function of particle thermal properties and slip temperature between particle and gas phases. In addition, ice crystal particle is assumed to be porous with its porosity factor adjusted by its melting behaviour [9]. Therefore, the initial ice core density (ρ_{core}) is dictated by the porosity factor (PF). During the melting stage, the ice core size gradually decreases and its density is assumed to be unchanged.

1. phase change model

Stage 1 ($T_{\mathrm{p}} < T_{\mathrm{m}}$): fully solid ice crystals $\rightarrow$ start of ice melting

$$m_{\mathrm{p}} c_{\mathrm{p,i}} \frac{\mathrm{d}T_{\mathrm{p}}}{\mathrm{d}t} = Q_{\mathrm{conv}} - \dot{m}_{\mathrm{sub}} L_{\mathrm{s}} \tag{1}$$

$$\frac{\mathrm{d}m_{\mathrm{p}}}{\mathrm{d}t} = -\dot{m}_{\mathrm{sub}} \tag{2}$$

$$Q_{\mathrm{conv}} = \frac{\pi D_{\mathrm{p}}}{\Phi} \mathrm{Nu}^{*} k_{\mathrm{g}} (T_{\mathrm{f}} - T_{\mathrm{p}}) \tag{3}$$

$$\dot{m}_{\mathrm{sub}} = \frac{\pi D_{\mathrm{p}}}{\Phi} \mathrm{Sh}^{*} \rho_{\mathrm{g}} D_{\mathrm{v,g}} (\gamma_{\mathrm{v,p}} - \gamma_{\mathrm{v,g}}) \tag{4}$$

$$T_{\mathrm{f}} = T_{\mathrm{g,s}} \left(1 + \mathrm{Pr}^{1/3} \frac{\gamma_{\mathrm{f}} - 1}{2} \mathrm{Ma}_{\mathrm{p,rel}}^{2} \right) \tag{5}$$

$$\rho_{\mathrm{core}} = (1 - \mathrm{PF}) \rho_{\mathrm{g}} + \mathrm{PF} \rho_{\mathrm{i}} \tag{6}$$

$$\rho_{\mathrm{p}} = \rho_{\mathrm{core}} \tag{7}$$

where, T_{p} is the particle temperature and T_{m} is the melting temperature ($273.15K$); $c_{\mathrm{p,i}}$ is the specific heat of the ice = $2108J/(kg.K)$, L_{s} is the total latent heat of fusion (L_{f}) and evaporation (L_{v}), Φ is the particle sphericity, Nu is the Nusselt number, k_{g} is the gas thermal conductivity, Sh is the Sherwood number, $D_{\mathrm{v,g}}$ is the water vapour diffusivity in the air, $\gamma_{\mathrm{v,p}}$ and $\gamma_{\mathrm{v,g}}$ are the vapour mass fraction at the particle surface and gas phase, respectively; T_{f} is the gas temperature local to the particle, $T_{\mathrm{g,s}}$ is the local gas static temperature, Pr is the Prandtl number, γ_{f} is the specific heat ratio, and $\mathrm{Ma}_{\mathrm{p,rel}}$ is the particle Mach number based on the slip velocity. When no slip ($\mathrm{Ma}_{\mathrm{p,rel}}$=0), T_{f}=$T_{\mathrm{g,s}}$. Porosity factor (PF), which is the particle porous property, represents the ratio of particle volume only occupied by ice. For

example, PF= 0.8 means 80% of particle volume is occupied by ice and 20% is occupied by air. ρ_{core} is the ice core density, which is used to calculate the density of ice particle. The effect of surface blowing on phase change, represented by $\mathrm{F_{SB}}$ (surface blowing factor), is caused by the influence of mass transfer at the particle surface of the local flowfield surrounding particles, which could be predicted by [20]:

$$\mathrm{F_{SB}} = \frac{1}{\left(1+\frac{(T_{\mathrm{g,s}}-T_{\mathrm{p}})C_{\mathrm{p,p}}}{L_{\mathrm{p}}}\right)^{0.7}} \tag{8}$$

$$C_{\mathrm{p,p}} = (1-\mathrm{MR})C_{\mathrm{p,i}} + \mathrm{MR} * C_{\mathrm{p,w}} \tag{9}$$

$$L_{\mathrm{p}} = (1-\mathrm{MR})L_{\mathrm{s}} + \mathrm{MR} * L_{\mathrm{v}} \tag{10}$$

where, $C_{\mathrm{p,p}}$ and L_{p} are the specific heat and the latent heat of the ice particles, MR is the particle melt ratio. In stage 1, the thermal properties are equal to the properties of ice; in stage 2, mass-averaged thermal properties are used; in the stage 3, the thermal properties are equal to the properties of water. Therefore, the Nusselt number and Sherwood number, $\mathrm{Nu^*}$ and $\mathrm{Sh^*}$, which considers the surface blowing, can be given by:

$$\frac{\mathrm{Nu^*}}{\mathrm{Nu}} = \mathrm{F_{SB}} \tag{11}$$

$$\frac{\mathrm{Sh^*}}{\mathrm{Sh}} = \mathrm{F_{SB}} \tag{12}$$

where, Nu and Sh are predicted by using the correlations derived by Villedieu et al. [3]:

$$\mathrm{Nu} = 2\sqrt{\varphi} + 0.55\mathrm{Pr}^{\frac{1}{3}}\varphi^{\frac{1}{4}}\sqrt{\mathrm{Re_p}} \tag{13}$$

$$\mathrm{Sh} = 2\sqrt{\varphi} + 0.55\mathrm{Sc}^{\frac{1}{3}}\varphi^{\frac{1}{4}}\sqrt{\mathrm{Re_p}} \tag{14}$$

where, Pr is the vapour Prandtl Number and Sc is the vapour Schmidt number.

Stage 2 ($T_{\mathrm{p}} = T_{\mathrm{m}}$): start of ice melting $\rightarrow$ 100% liquid

$$Q_{\mathrm{conv}} = \dot{m}_{\mathrm{evap}}L_{\mathrm{v}} + \dot{m}_{\mathrm{melt}}L_{\mathrm{f}} \tag{15}$$

$$\frac{\mathrm{d}m_{\mathrm{p}}}{\mathrm{d}t} = -\dot{m}_{\mathrm{evap}} \tag{16}$$

$$\frac{\mathrm{d}m_{\mathrm{p,i}}}{\mathrm{d}t} = -\dot{m}_{\mathrm{melt}} \tag{17}$$

$$m_{\mathrm{p,w}} = m_{\mathrm{p}} - m_{\mathrm{p,i}} \tag{18}$$

$$\dot{m}_{\mathrm{evap}} = \frac{\pi D_{\mathrm{p}}}{\Phi}\mathrm{Sh^*}\rho_{\mathrm{g}}D_{\mathrm{v,g}}(\gamma_{\mathrm{v,p}} - \gamma_{\mathrm{v,g}}) \tag{19}$$

$$\rho_{\mathrm{p}} = 1/\left(\frac{1-\mathrm{MR}}{\rho_{\mathrm{core}}} + \frac{\mathrm{MR}}{\rho_{\mathrm{w}}}\right) \tag{20}$$

where, the subscripts i and w represent ice and water, respectively. Therefore, the particle melt ratio is given by:

$$\mathrm{MR} = \frac{m_{\mathrm{p,w}}}{m_{\mathrm{p}}} \tag{21}$$

According to the assumption of particle sphericity being linearly dependent with the MR [3], particle sphericity is given by:

$$\Phi = \mathrm{MR}(1 - \Phi_0) + \Phi_0 \tag{22}$$

where, Φ_0 is the initial particle sphericity.

Stage 3 ($T_{\mathrm{p}} > T_{\mathrm{m}}$): 100% liquid

$$m_{\mathrm{p}} c_{\mathrm{p,w}} \frac{\mathrm{d}T_{\mathrm{p}}}{\mathrm{d}t} = Q_{\mathrm{conv}} - \dot{m}_{\mathrm{evap}} L_{\mathrm{v}} \tag{23}$$

$$\frac{\mathrm{d}m_{\mathrm{p}}}{\mathrm{d}t} = -\dot{m}_{\mathrm{evap}} \tag{24}$$

$$\rho_{\mathrm{p}} = \rho_{\mathrm{w}} \tag{25}$$

B. Wet bulb temperature

Wet bulb temperature (WBT), which is the temperature of moist air cooled to saturation under adiabatic evaporative-cooling process [21, 22], is as a function of temperature, pressure and humidity. Therefore, derivation of WBT is based on analysing the adiabatic evaporative-cooling process of moist air from unsaturation to saturation [21, 22]. The equations needed to evaluate the adiabatic evaporative-cooling process is:

$$h_{0,\mathrm{Ts}} + (\Omega_{\mathrm{s,WBT}} - \Omega_{0,\mathrm{Ts}}) h_{\mathrm{w,WBT}} = h_{\mathrm{s,WBT}} \tag{26}$$

where, $h_{0,\mathrm{Ts}}$ and $h_{\mathrm{s,WBT}}$ are the specific enthalpies of moist air evaluated at the static air temperature and the wet bulb temperature in $^{\circ}C$ *, respectively; $h_{\mathrm{w,WBT}}$ is the specific enthalpy of water added to moist air evaluated at the wet bulb temperature; $\Omega_{0,\mathrm{Ts}}$ is the humidity ratio of moist air at the static air temperature and $\Omega_{\mathrm{s,WBT}}$ is the saturated humidity ratio of moist air at the wet bulb temperature.

$$h_{0,\mathrm{Ts}} = h_{\mathrm{da,Ts}} + \Omega_{0,\mathrm{Ts}} h_{\mathrm{wv,Ts}} \tag{27}$$

$$h_{\mathrm{s,WBT}} = h_{\mathrm{da,WBT}} + \Omega_{\mathrm{s,WBT}} h_{\mathrm{wv,WBT}} \tag{28}$$

$$h_{\mathrm{w,WBT}} = 4.186\mathrm{WBT} \tag{29}$$

*The convention is that the variable after the comma in the subscript means 'evaluated at that temperature'.

where, $h_{\mathrm{da,Ts}}$ and $h_{\mathrm{da,WBT}}$ are the specific enthalpies of dry air in kJ/kg evaluated at the static air temperature and the wet bulb temperature using Equation (30), respectively; $h_{\mathrm{wv,Ts}}$ and $h_{\mathrm{wv,WBT}}$ are the specific enthalpies of saturated water vapour in kJ/kg evaluated at the static air temperature and the wet bulb temperature using Equation (31), respectively.

$$h_{\mathrm{da}} = 1.006T \tag{30}$$

$$h_{\mathrm{wv}} = 2501 + 1.805T \tag{31}$$

where, T will be Ts and WBT.

Therefore, Equation (26) can be rewritten into Equation (32) by substituting the terms of the specific enthalpies and the humidity ratios:

$$\mathrm{WBT} = \frac{2501\Omega_{\mathrm{s,WBT}} - (1.006Ts + (2501 + 1.805Ts)\Omega_{0,\mathrm{Ts}})}{2.381\Omega_{\mathrm{s,WBT}} - 4.186\Omega_{0,\mathrm{Ts}} - 1.006} \tag{32}$$

$$\Omega_{0,\mathrm{Ts}} = 0.62198\frac{\mathrm{RH}P_{\mathrm{s,Ts}}}{Ps - \mathrm{RH}P_{\mathrm{s,Ts}}} \tag{33}$$

$$\Omega_{\mathrm{s,WBT}} = 0.62198\frac{P_{\mathrm{s,WBT}}}{Ps - P_{\mathrm{s,WBT}}} \tag{34}$$

where, RH is the relative humidity; $P_{\mathrm{s,Ts}}$ and $P_{\mathrm{s,WBT}}$ are the saturation pressures of water vapor at Ts and WBT, respectively; Ps is the static pressure of moist air. It can be found that only WBT is unknown in Equation (32), which can be solved iteratively. Fig. 1 shows that the predicted WBT in this study is close to the reference WBT from [23], which was derived in a similar way to this study.

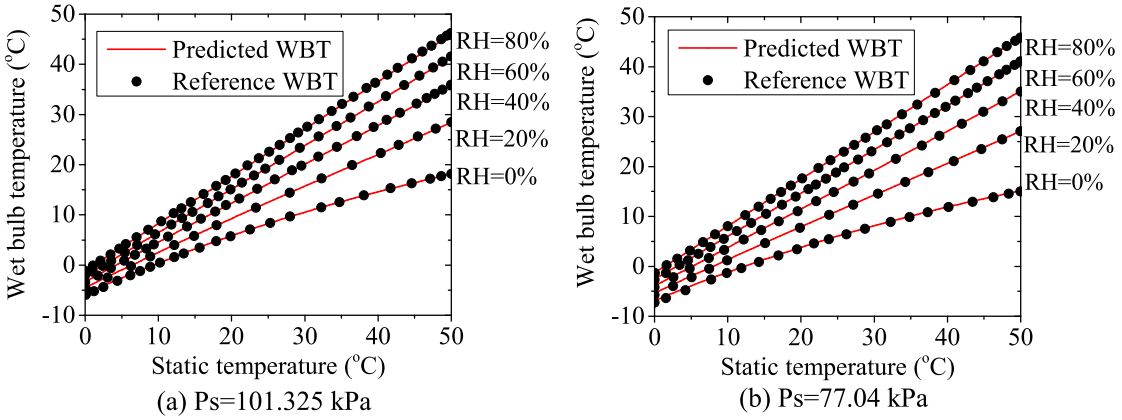

Fig. 1 Comparison of the predicted WBT and the reference WBT as a function of temperature and humidity for pressures at (a)101.325 kPa and (b) 77.04 kPa.

IV. Evaluation test description

The melting behaviours of ice particles were investigated by Hauk et al [13, 14]. The purpose of the experiments was to improve the understanding of the melting behaviour of single ice particles, as well as providing a database for the validation of ice melting models. The tests were mainly carried out by: (i) suspending ice particles in a chest freezer via an acoustic levitator; (ii) blowing air flow through the ice particle at a specified velocity, temperature and humidity; and (iii) recording the images of ice particles during the melting process using an optical system. The experimental melting time was determined at the time point when the ice core had just disappeared. Multiple operation conditions were tested at varied flow temperature, flow velocity, relatively humidity, and initial ice temperature. The 8 sets of experimental data, which are detailed in reference [13], are used for model evaluation in this study. The operation conditions (including pressure-P_{g}, temperature-T_{g},velocity-V_{g}, and RH), ice particle properties (including mass-m_{p}, temperature-T_{p}, and the projected areas-$A_{\max}$ and $A_{\min}$) and the experimental melting time ($T_{\mathrm{melt,exp}}$) are complied in Tables (1) and (2). Particle Number 3 and 4 are spherical particles and all others are non-spherical particles. It should be noted that data for the particle mass and melting time were obtained from the figures in reference [13]. In addition, particle projected areas were processed from the ice images presented in reference [13] using the image area function ('bwarea') in Matlab. All other data in the two tables are drawn directly from reference [13]. Volume equivalent particle size, D_{p}, is derived from the particle mass and ice density. For comparison, the following sphericities (Φ) of the non-spherical particles (number 1, 2, and 5-8) are derived using Equations (35) to (40): (i) mean sphericity, Φ_{m}, which is assumed to be equal to the mean value of the cross sphericities [13]; (ii) prolate sphericity, Φ_{p}, which assumes prolate shape; (iii) oblate sphericity, Φ_{o}, which assumes oblate shape. Table (3) shows the estimated sphericities. These experimental data are employed to calculate the error bars of the predicted melting time. The mean relative difference (MRD) between the predictions and measurements is defined by Equation (41).

$$\Phi_{\mathrm{m}} = \frac{1}{2}\left(\frac{\pi D_{\mathrm{p}}^2}{4A_{\max}} + \frac{\pi D_{\mathrm{p}}^2}{4A_{\min}}\right) \tag{35}$$

$$\Phi_{\mathrm{p}} = \frac{2\mathrm{E}_{\mathrm{p}}^{2/3}}{1 + \mathrm{E}_{\mathrm{p}}\frac{\arcsin(e)}{e}} \tag{36}$$

$$\Phi_{\mathrm{o}} = \frac{4\mathrm{E}_{\mathrm{o}}^{2/3}}{2 + \frac{\mathrm{E}_{\mathrm{o}}^2}{e}\ln\left(\frac{1+e}{1-e}\right)} \tag{37}$$

$$\mathrm{E}_{\mathrm{p}} = \left(\frac{\pi D_{\mathrm{p}}^2}{4A_{\max}}\right)^{-3} \tag{38}$$

$$\mathrm{E}_{\mathrm{o}} = \left(\frac{\pi D_{\mathrm{p}}^2}{4A_{\max}}\right)^{3/2} \tag{39}$$

$$e = \sqrt{1 - \min(\mathrm{E}, 1/\mathrm{E})^2} \tag{40}$$

$$\mathrm{MRD} = \left(\sum_{\mathrm{i}=1}^{\mathrm{n}} \frac{\mid t_{\mathrm{melt,exp,i}} - t_{\mathrm{melt,pred,i}} \mid}{t_{\mathrm{melt,exp,i}}}\right)/n \tag{41}$$

Table 1 Operating conditions of the tests.

No.	P_g, **bar**	T_g, $^\circ C$	V_g, **m/s**	RH, **%**
1	0.96 ± 0.0014	20 ± 0.3	$1 \pm 5\%$	4 ± 1
2	0.96 ± 0.0014	20 ± 0.3	$1 \pm 5\%$	4 ± 1
3	0.95 ± 0.0014	15 ± 0.3	$0.75 \pm 5\%$	62 ± 5
4	0.95 ± 0.0014	20 ± 0.3	$1 \pm 5\%$	73 ± 5
5	0.95 ± 0.0014	20 ± 0.3	$1 \pm 5\%$	73 ± 5
6	0.95 ± 0.0014	20 ± 0.3	$1 \pm 5\%$	73 ± 5
7	0.95 ± 0.0014	20 ± 0.3	$1 \pm 5\%$	73 ± 5
8	0.95 ± 0.0014	20 ± 0.3	$1 \pm 5\%$	73 ± 5

Table 2 Particle relevant properties and melting time of the tests.

No.	m_p, ng	T_p, $^\circ C$	A_{max}, mm^2	A_{min}, mm^2	$T_{melt,exp}$, s
1	$96 \pm 9.2\%$	-17 ± 0.5	0.38	0.27	12.5 ± 0.4
2	$192 \pm 9.2\%$	-17 ± 0.5	0.63	0.39	16.7 ± 0.4
3	$803 \pm 3.7\%$	-17 ± 0.5	0.41	0.41	13.3 ± 0.4
4	$452 \pm 2.7\%$	-18 ± 0.5	0.69	0.69	10.3 ± 0.4
5	$327 \pm 2.7\%$	-18 ± 0.5	0.84	0.71	6.0 ± 0.4
6	$233 \pm 2.7\%$	-18 ± 0.5	0.69	0.50	5.7 ± 0.4
7	$78 \pm 2.7\%$	-18 ± 0.5	0.36	0.19	3.1 ± 0.4
8	$192 \pm 2.7\%$	-18 ± 0.5	0.80	0.59	4.3 ± 0.4

Table 3 Estimated particle sphericities that were used in the melting models.

	1	2	3	4	5	6	7	8
Φ_m	0.83	0.83	1	1	0.78	0.81	0.86	0.61
Φ_p	0.87	0.83	1	1	0.87	0.85	0.81	0.67
Φ_o	0.95	0.94	1	1	0.95	0.95	0.93	0.84

V. Results and discussion

A. Model Evaluation

Figure 2(a)[†] shows the measured and predicted ice melting time with the assumptions of spherical shape and non-spherical shape based on the mean sphericity, Φ_m. The measured melting times of particle numbers from 4 to

[†]The comparison of the predicted melting times is based on the same experimental melting times.

8, where the flow conditions were identical to each other except for particle mass and sphericity, are in the order of $T_{\mathrm{melt},4} > T_{\mathrm{melt},5} > T_{\mathrm{melt},6} > T_{\mathrm{melt},8} > T_{\mathrm{melt},7}$. This is because the rate of change of temperature ($\frac{\mathrm{d}T_\mathrm{p}}{\mathrm{d}t}$) in the heat equation is positively related to the term of surface area-to-mass, $F_{\mathrm{a2m}} = D_\mathrm{p}/(\Phi m_\mathrm{p}) \propto 1/(\Phi m_\mathrm{p}^{2/3})$. The term is in the order of $F_{\mathrm{a2m},4} < F_{\mathrm{a2m},5} < F_{\mathrm{a2m},6} < F_{\mathrm{a2m},8} < F_{\mathrm{a2m},7}$, which is in accordance with the order of the measured melting times. In addition, the measured melting times of particle number 1 and 2, where the particle mass and sphericity are close to particle number 7 and 8, are approximately four times those of particle number 7 and 8, respectively. This is because RH is 4% for particle number 1 and 2 while it is 73% for particle number 7 and 8. Low humidity can promote evaporative cooling, which can increase melting time. It is noted that the predictions correctly capture these experimental melting observations. Fig. 2(a) also shows that the spherical assumption tends to overestimate the melting time of non-spherical particles and the mean relative difference (MRD) is approximately 16.4%. With the assumption of non-spherical shape, the mean relative difference reduces to 10.6%. This is comparable to the modelling results presented by Hauk et al.[13], where the difference reduced from 19.9% to 9.7% by replacing the spherical assumption with the non-spherical assumption.

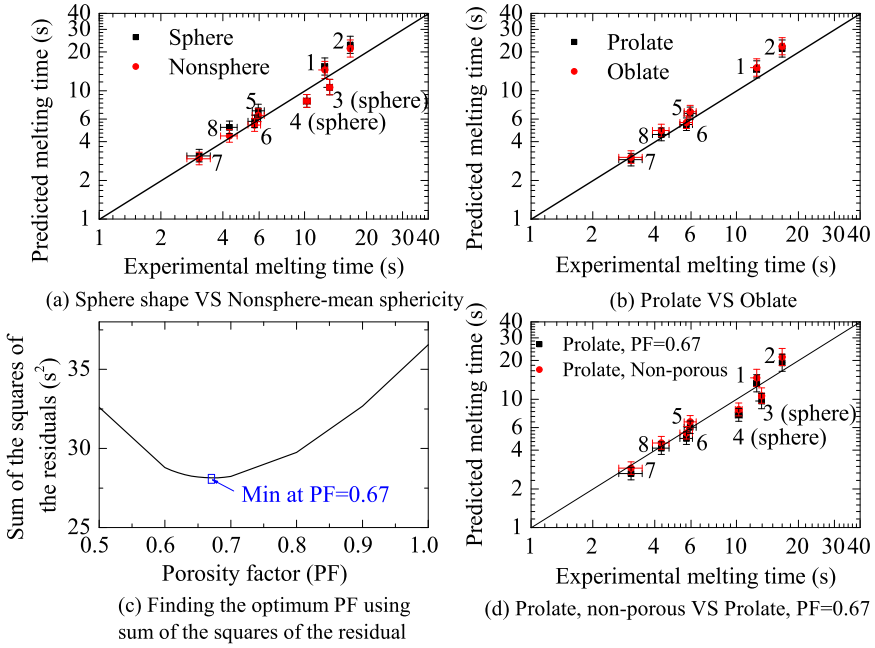

Fig. 2 Measured and predicted melting time: (a) spherical VS non-spherical; (b) prolate VS oblate; (c) the optimum PF; (d) Non-porous VS PF=0.67.

In an icing code, it may be necessary to assume a regular non-spherical shape for ice particles for particle tracking. This is because the empirical correlations of drag force, lift force and torques are often derived based on regular particle shapes. In this study, ice particles are assumed to be spheroids since the approach solely uses aspect ratio to define the non-spherical shape [9]. In addition, the relevant empirical correlations used for particle tracking can be found for spheroid particles in the literature [24–26]. Fig. 2(b) shows the measured and predicted ice melting times with the

assumptions of prolate and oblate. The mean relative difference reduces from 16.4% to 11.9% and 14.1% after the ice shape is changed from sphere to prolate and oblate, respectively. This indicates that the predicted melting times are closer to the experimental data compared to the spherical assumption. The prolate shape [‡] shows relatively better predictions compared to oblate shape for the data used in this study. This is because the derived sphericity of the prolate shape is relatively smaller than that of the oblate shape shown in Table (3), which leads to relatively lower predictions of melting time. The mean relative difference of melting time with the non-spherical assumptions is still noticeable (10.6% for mean sphericity and 11.9% for the prolate assumption). This could be due, not only to the deviation of the real irregular ice shape from the assumed non-spherical shape, but also to the porosity of ice particles. Since the real ice porosity is unknown, an optimized numerical porosity factor with a value of 0.67 [§] is determined by using the least square methods as shown in Fig. 2(c). Fig. 2(d) shows that the mean melting time reduces by approximately 9.3% after using the optimized porosity factor. The mean relative difference reduces from 11.9% to 8.8% for non-spherical particles and from 13.8% to 13.3% for all 8 particles. This implies that using the porous assumption might have the potential to reduce the overestimation of the ice melting time of non-spherical particles.

The effect of surface blowing on ice melting behaviour is often neglected in most existing ice melting models. Fig. 3 shows the trend of the surface blowing factor (F_{SB}) during the ice melting process for particle number 1 [¶]. It can be observed that the trend of the surface blowing factor is in accordance with the change in the particle temperature. In stage 1, where the ice particle is still fully solid, the effect of surface blowing, represented by $(1 - F_{SB}) * 100$, decreases with the raise in the particle temperature. This is because the temperature difference drops with the increase in particle temperature. In stage 2, where the ice particle is partially melted, the effect of surface blowing increases due to the ice particle gradually melting and the mean thermal property tends to be closer to a water droplet. In stage 3, where the ice particle is fully melted, the effect of surface blowing decreases again due to the increase in particle temperature. The effect of surface blowing, ranging from 1% to 2.3%, is quite close to zero. As a result, there is a small effect of surface blowing on particle melting time. The mean melting time with surface blowing is approximately 1.6% more than that without surface blowing. As the surface blowing factor is influenced by gas temperature, the effect of gas temperature on surface blowing is investigated and as shown in Fig. 4. It can be seen that the effect of surface blowing increases approximately linearly with the increase in gas temperature. This is because increasing the gas temperature can raise the temperature difference between particle and gas as shown in Equation (8). As a result, the mean relative difference of melting time between surface blowing and no surface blowing increases from 1.6% to 3.2% and 6.9% by increasing gas temperature from 20 $^{\circ}C$ to 40 and 90 $^{\circ}C$. This suggests that neglecting surface blowing cannot obviously affect the predictions of melting behaviour for fundamental icing tests, where the operation temperature is often below 40 $^{\circ}C$ [17, 18, 27, 28]. However, surface blowing may still need to be considered for engine conditions, where the gas

[‡]In this study, if the shape assumption is not mentioned, the assumption of a prolate shape is used in the modellings by default.
[§]The value of 0.67 represents 67% of total particle volume is occupied by ice.
[¶]Particle number 1 is taken as an example and other particles show a similar behaviour.

temperature in compressor could be higher than 100 $^{\circ}C$ [13].

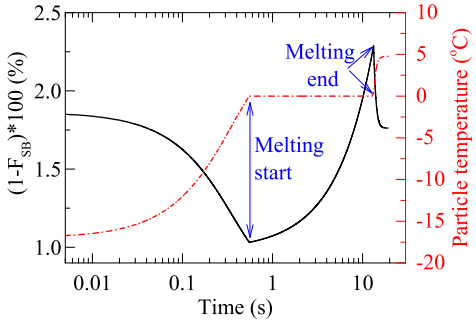

Fig. 3 The surface blowing factor during ice melting of particle number 1.

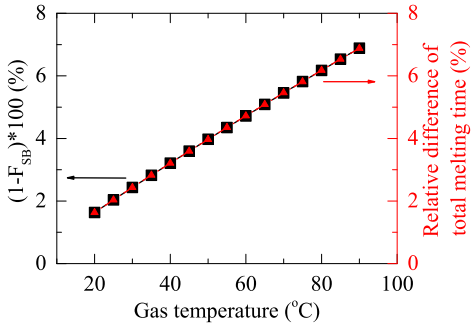

Fig. 4 The effect of gas temperature on the mean surface blowing factor and melting time of particle number 1.

B. Parametric study

The present ice melting model is employed to investigate the effects of flow conditions and particle properties on ice melting time. Compared to the sizes (ranging from approximately 500 μm to 1000 μm) in Hauk's melting data [13], much smaller particle sizes (approximately 15-100 μm), which are closer to engine icing conditions, are used for the parametric study. The ice melting model should be valid for smaller particles as the Biot number ($= \frac{h_t(D_p/6)}{k_p} = \frac{\mathrm{Nu}k_g}{6k_p}$) is much smaller than 0.1, the criterion for using the lumped ice melting model [29]. Table 4 lists the parameters used in the parametric study. Two baseline cases with low and high humidities (RH = 15% and 70%) are considered as evaporation and sublimitation are dependent on humidities.

1. Flow conditions

Figures 5(a) shows the effect of total pressure on ice melting behaviours. Particle melting time increases with pressure at high humidity while the melting time decreases with pressure at low humidity. This can be explained by the phase change behaviour. The mass flux of phase change reduces with the increase in the pressure. At low humidity,

Table 4 The parameters used in the parametric study.

	Parameter	Baseline low RH	Baseline high RH	Range
Flow conditions	P0, kPa	50	50	[34.5, 101.325]
	T0, $°C$	30	30	[10,50]
	RH	0.15	0.7	[0.15,1]
	V_{slip}, m/s	1	1	[0.01,100]
	Ma	0.3	0.3	[0.1,0.6]
Particle properties	D_p, μm	40	40	[15,100]
	AR	3	3	[1,10]
	PF	0.67	0.67	[0.5,1]
	$T_{\text{p,0}}$,$°C$	-20	-20	[-50,-1]

strong sublimation and evaporation occurs during ice melting. This contributes to heat loss for particles. As a result, the heat loss reduces due to the decrease in the mass flux of phase change when increasing the pressure. Therefore, particle melting time decreases with pressure. At high humidity, water vapour transfers from gas to particles according to the mass transfer equation (4) and (19), which contributes to heat gain for particles. Hence, the heat gain can reduce with pressure due to the reduction in the mass flux. As a result, particle melting time increases with pressure at high humidity. Fig. 5(b) and (c) shows the effect of humidity and total temperature on ice melting time. Particle melting time decreases with an increase in either of the two flow conditions. This is because convective heat transfer increases with temperature and the heat gained from phase change increases with humidity. Fig. 5(d) shows the effect of Mach number on melting behaviours. Mach number is considered by its effect on static gas temperature and pressure. Increasing Ma can decrease static temperature and pressure. At low humidity, both the heat from convective heat transfer and phase change reduces. At high humidity, the heat from convective heat transfer reduces while the heat gained from phase change increases. However, the overall heat gained reduces so the melting time is still increasing at high humidity. In addition, it can be observed that at high humidity, the melting time increases at a slower rate compared to low humidity. The melting times increase by 50% and 420% at high humidity and low humidity, respectively, by increasing the Mach number from 0.1 to 0.35. Fig. 5(e) shows the effect of slip velocity on particle melting time. It can be observed that the melting time quickly reduces with slip velocity. The melting times reduce by 84% and 98% at the high humidity and low humidity, respectively, by increasing the slip velocity from 1 to 100 m/s. Increasing the slip velocity can increase the particle Reynolds numbers, which can increase Nusselt number and Sherwood number. As a result, the particle melting time reduces. This implies that non-uniform flow, which can increase the particle Reynolds number, can promote the heat and mass transfer during ice melting.

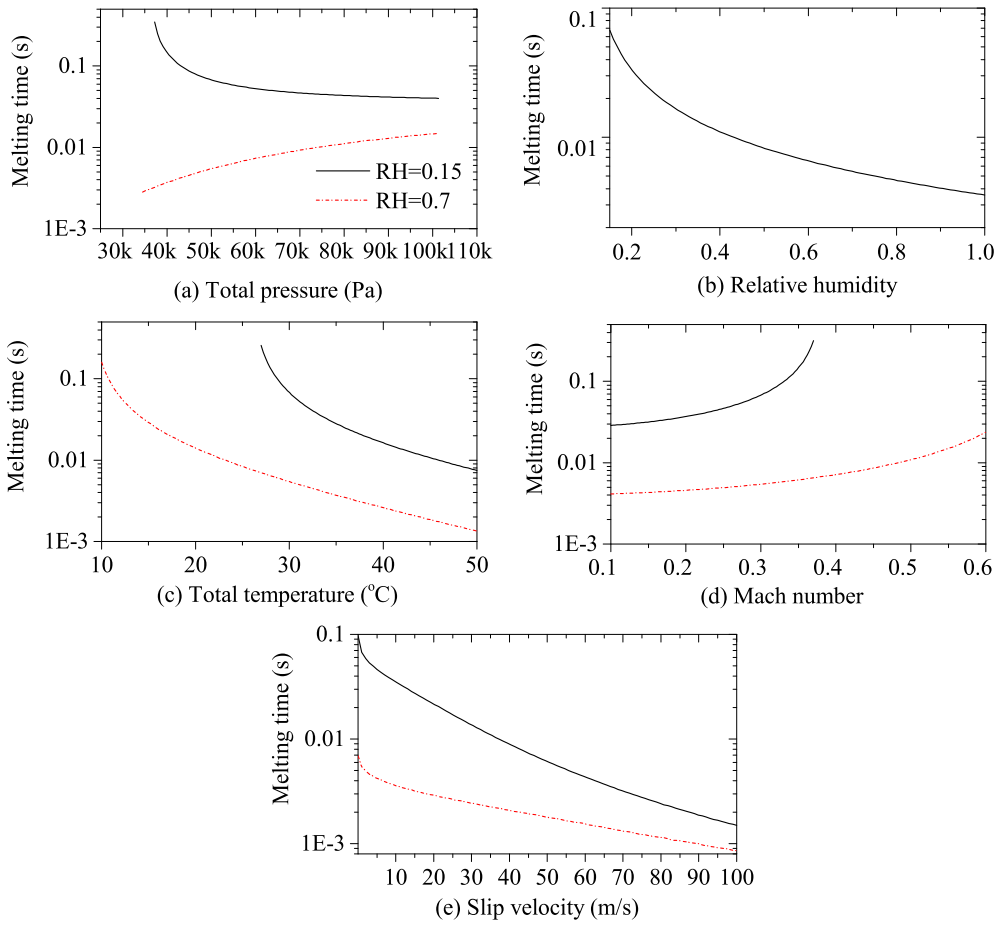

Fig. 5 The effect of flow conditions on ice melting behaviour: (a) total pressure; (b) relative humidity; (c) total temperature; (d) Mach number; (e) slip velocity.

The wet bulb temperature is often used to evaluate the melting potential of ice particles. Fig. 6 shows the melting time as a function of the wet bulb temperature for the numerical data presented in Fig. 5. First, melting time decreases with the increase in the wet bulb temperature for most scenarios. However, in a scenario where the pressure is varied at high humidity the opposite trend (the red curve) is seen. This is because the wet bulb temperature is defined under the assumption that the water vapour phase evaporates from the water liquid phase into air in order to make the air reach saturation. As a result, the wet bulb temperature always increases with pressure. However, at high humidity, the water vapour may transfer from the air to the ice particles. As mentioned in Fig. 5(a), under this scenario, particle melting time increases with the increase in pressure even though the wet bulb temperature increases. Secondly, there might be risk involved in only using the wet bulb temperature to evaluate the melting potential under multiple varied flow conditions, as the curves do not coincide with each other especially within the lower bounds of the wet bulb temperature. For example, at the WBT of 9 $^{\circ}C$, the corresponding melting times of each scenario are in a rank of Ma-high RH<T-high RH<RH<T-low RH<Ma-low RH<P-low RH. The ratio of the highest to the lowest melting time among these scenarios

is approximately three times. However, it is still acceptable to employ the WBT to rank melting potential when only one flow condition is changed. This is because all the melting time-WBT curves vary monotonically. In addition, it is noted that, if both pressure and humidity are held as constants, the melting time-WBT curves almost coincides under the scenarios of total temperature and Mach number when WBT is the same as shown in Fig. 7. This suggests that the WBT could be used to evaluate the melting potential for a varied total temperature and Mach number.

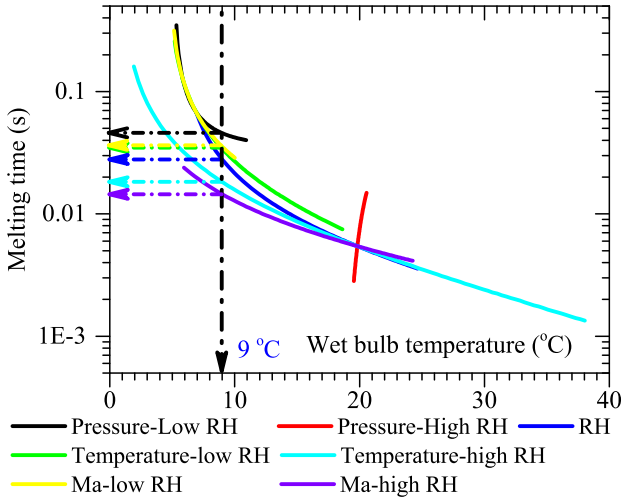

Fig. 6 Melting time as a function of wet bulb temperature using the numerical data presented in Fig. 5.

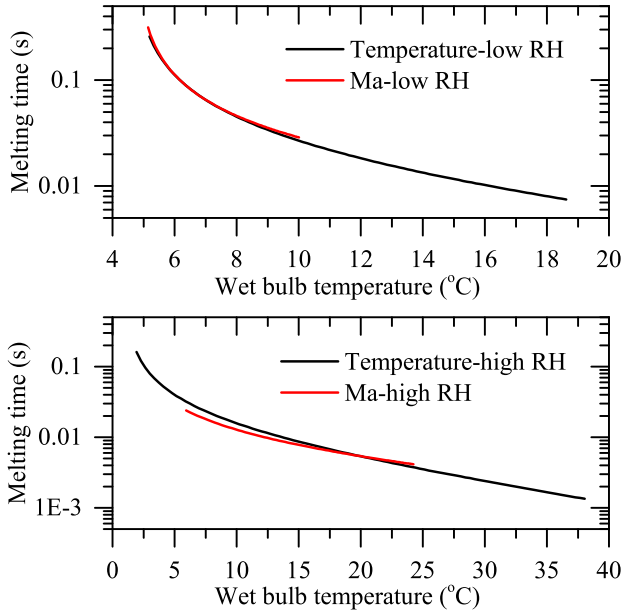

Fig. 7 Melting time as a function of wet bulb temperature for conditions varying temperature and Mach number.

2. Particle properties

Figure 8 shows the effect of particle size, aspect ratio, porosity factor and particle initial temperature on ice melting time. It can be observed that increasing the size and porosity factor can increase the melting time while increasing aspect ratio and particle initial temperature can reduce the melting time. It is observed that increasing aspect ratio from 1 to 10 (correspondingly, sphericity reduces from 1 to 0.6), the melting time reduced by approximately 13-14%, while increasing particle size from 15 to 100 increases the melting time by approximately 3000-3400%. Reducing the porosity factor ‖ from 1 to 0.9, 0.8, 0.67 and 0.5 leads to a decrease in the melting time by approximately 8%, 17%, 28% and 44%, respectively. This implies that when the particle size and shape are held as constants, assuming porous ice particles can efficiently enhance the melting potential. For existing fundamental ice accretion tests, the mass of ice crystal particles is often not directly measured, but derived from images of ice particles [30]. Hence, it is needed to further validate the current assumption of porous ice particles for fundamental icing tests in wind tunnels. Also, increasing the particle initial temperature from -50 to -1 $°C$ decreases the melting time by approximately 5.4% and 16.3% for low and high humidities, respectively. This implies that the effect of particle initial temperature on melting behaviour is sensitive to humidity.

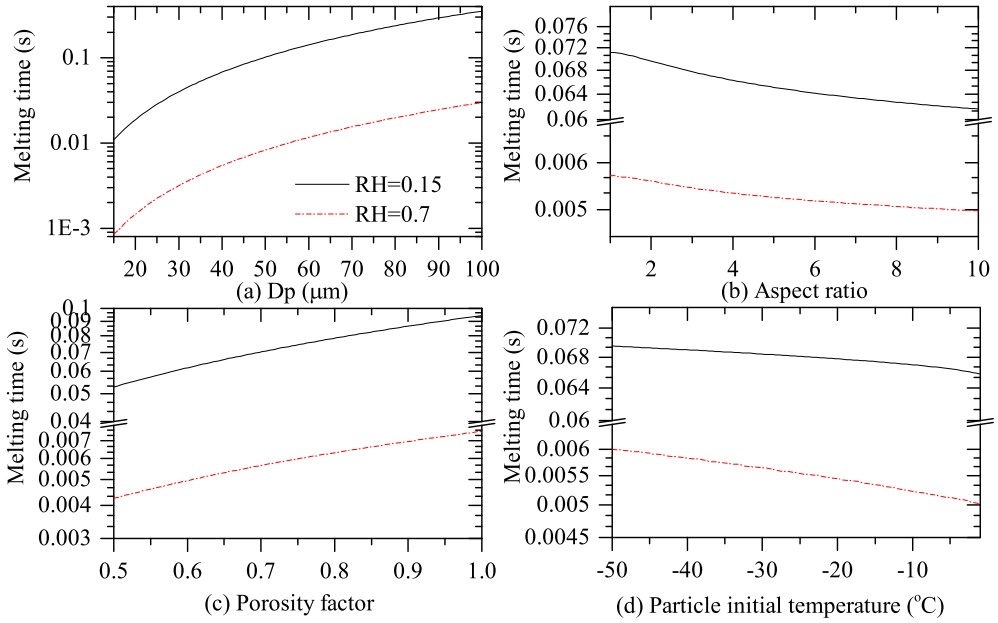

Fig. 8 The effect of particle properties on ice melting behaviour: (a) particle size; (b) aspect ratio; (c) porosity factor; (d) particle initial temperature.

It is useful to derive an index that can be used to quickly evaluate the melting potential based on particle geometric parameters (size, shape and PF). As mentioned in Section A, the rate of change of temperature ($\frac{dT_p}{dt}$) in Equation (1) is positively related to the term, $D_p/(\Phi m_p)$. By multiplying this term with Nu and replacing m_p with D_p^3, an index can

‖ In this section, porosity factor is included via its effect on ice core density as shown in Equation 6 while particle size and shape are held as constants.

be $\mathrm{Nu}/(\Phi * D_{\mathrm{p}}^2)$. Fig. 9 shows the melting time as a function of the index, $\mathrm{Nu}/(\Phi * D_{\mathrm{p}}^2)$. It can be observed that the melting time gradually decreases with an increase of the index. Also, the curves for each of the particle parameters are quite close to each other especially between the particle size and particle aspect ratio while the slope for the porosity factor is different from the other two parameters. This implies that if the flow conditions and porosity factor are held as constants, the index, $\mathrm{Nu}/(\Phi * D_{\mathrm{p}}^2)$, could be useful for evaluating the melting potential of ice particles.

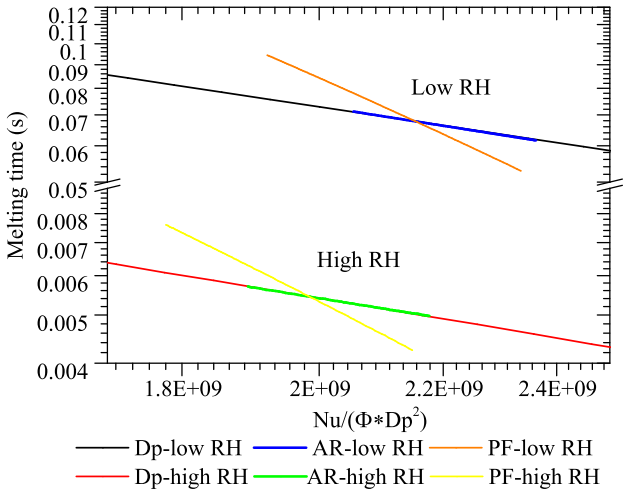

Fig. 9 Melting time as a function of the factor, $\mathrm{Nu}/(\Phi * D_{\mathrm{p}}^2)$, for conditions varying D_{p}, AR, and PF using the numerical data presented in Fig. 8.

VI. Conclusions

1) An ice melting model integrated with surface blowing and porosity has been developed to model the phase change behaviour of ice crystals. The model has been compared against the melting behaviour of single ice particles in an acoustic levitator. Considering sphericity and porosity can improve prediction performance. The effect of surface blowing on ice melting increases with gas temperature. Ignoring surface blowing would not obviously affect the accuracy of predictions for fundamental icing tests as the gas temperature is often below 40 $^{\circ}C$ while the effect might need be considered for high gas temperature conditions.
2) The parametric study shows that the ice melting model is able to take into account the main factors (flow conditions and particle properties) in dictating the melting behaviour of ice particles. The effect of pressure on ice melting is related to humidity. Ice melting time increases with pressure at high humidity while an opposite trend is observed at low humidity. Increasing gas temperature, humidity, slip velocity, aspect ratio, and particle temperature can decrease ice melting time while increasing Mach number, particle size, and porosity factor can increase ice melting time.
3) The wet bulb temperature can be used to evaluate ice melting potential when only one flow parameter is varied. However, one should be cautious when employing the wet bulb temperature under scenarios where multiple flow

parameters are varied. The index, $\mathrm{Nu}/(\Phi * D_{\mathrm{p}}^2)$, can be used as an indicator of particle melting potential for particles with different size and sphericity under the same flow conditions and porosity factor.

Acknowledgments

The authors would like to acknowledge Rolls-Royce and the Aerospace Technology Institute (ATI) for funding provided within their De-ICER programme which supported this research.

References

[1] Mason, J., Strapp, W., and Chow, P., "The ice particle threat to engines in flight," *44th AIAA Aerospace Sciences Meeting and Exhibit*, AIAA Paper 2002-0206, Jan. 2006. https://doi.org/10.2514/6.2006-206.

[2] Wright, W., Jorgenson, P., and Veres, J., "Mixed phase modeling in GlennICE with application to engine icing," *AIAA Atmospheric and Space Environments Conference*, AIAA Paper 2010-7674, Jun. 2010, p. 7674. https://doi.org/10.2514/6.2010-7674.

[3] Villedieu, P., Trontin, P., and Chauvin, R., "Glaciated and mixed phase ice accretion modeling using ONERA 2D icing suite," *6th AIAA Atmospheric and Space Environments Conference*, AIAA Paper 2014-2199, Jun. 2014. https://doi.org/10.2514/6.2014-2199.

[4] Radenac, E., Bayeux, C., and Villedieu, P., "Use of a Two-Dimensional Finite Volume Integral Boundary-Layer Method for Ice-Accretion Calculations," *AIAA Journal*, Vol. 58, No. 4, 2020, pp. 1592–1606. https://doi.org/10.2514/1.J058701.

[5] Ayan, E., and Özgen, S., "In-flight ice accretion simulation in mixed-phase conditions," *The Aeronautical Journal*, Vol. 122, No. 1249, 2018, pp. 409–441. https://doi.org/10.1017/aer.2017.127.

[6] Habashi, W., and Nilamdeen, S., "Multiphase approach toward simulating ice crystal ingestion in jet engines," *Journal of Propulsion and Power*, Vol. 27, No. 5, 2011, pp. 959–969. https://doi.org/10.2514/1.B34059.

[7] Norde, E., van der Weide, E. T. A., and Hoeijmakers, H. W. M., "Eulerian Method for Ice Crystal Icing," *AIAA journal*, Vol. 56, No. 1, 2017, pp. 222–234. https://doi.org/10.2514/1.J056184.

[8] Norde, E., Senoner, J.-M., van der Weide, E. T. A., Trontin, P., Hoeijmakers, H. W. M., and Villedieu, P., "Eulerian and Lagrangian Ice-Crystal Trajectory Simulations in a Generic Turbofan Compressor," *Journal of Propulsion and Power*, Vol. 35, No. 1, 2019, pp. 26–40. https://doi.org/10.2514/1.B36916.

[9] Bucknell, A., McGilvray, M., Gillespie, D., Yang, X., Jones, G., and Collier, B., "ICICLE: A Model for Glaciated & Mixed Phase Icing for Application to Aircraft Engines," *International Conference on Icing of Aircraft, Engines, and Structures*, SAE Paper 2019-01-1969, Jun. 2019. https://doi.org/10.4271/2019-01-1969.

[10] Mason, B. J., "On the melting of hailstones," *Quarterly Journal of the Royal Meteorological Society*, Vol. 82, No. 352, 1956, pp. 209–216. https://doi.org/10.1002/qj.49708235207.

[11] Rasmussen, R., and Pruppacher, H. R., "A Wind Tunnel and Theoretical Study of the Melting Behavior of Atmospheric Ice Particles. I: A Wind Tunnel Study of Frozen Drops of Radius < 500μm," *Journal of the Atmospheric Sciences*, Vol. 39, No. 1, 1982, pp. 152–158. https://doi.org/10.1175/1520-0469(1982)039<0152:AWTATS>2.0.CO;2.

[12] Rasmussen, R. M., Levizzani, V., and Pruppacher, H. R., "A Wind Tunnel and Theoretical Study of the Melting Behavior of Atmospheric Ice Particles. II: A Theoretical Study for Frozen Drops of Radius < 500μm," *Journal of the Atmospheric Sciences*, Vol. 41, No. 3, 1984, pp. 374–380. https://doi.org/10.1175/1520-0469(1984)041<0374:AWTATS>2.0.CO;2.

[13] Hauk, T., Roisman, I. V., and Tropea, C. D., "Investigation of the Melting Behaviour of Ice Particles in an Acoustic Levitator," *11th AIAA/ASME Joint Thermophysics and Heat Transfer Conference*, AIAA Paper 2014-2261, Jun. 2014. https://doi.org/10.2514/6.2014-2261.

[14] Hauk, T., Bonaccurso, E., Villedieu, P., and Trontin, P., "Theoretical and experimental investigation of the melting process of ice particles," *Journal of Thermophysics and Heat Transfer*, Vol. 30, No. 4, 2016, pp. 946–954. https://doi.org/10.2514/1.T4886.

[15] Currie, T., Fuleki, D., and Davison, C., "Simulation of Ice Particle Melting in the NRCC RATFac Mixed-Phase Icing Tunnel," *SAE 2015 International Conference on Icing of Aircraft, Engines, and Structures*, SAE Paper 2015-01-2107, Jun. 2015. https://doi.org/10.4271/2015-01-2107.

[16] Struk, P., Bartkus, T., Tsao, J.-C., Currie, T., and Fuleki, D., "Ice Accretion Measurements on an Airfoil and Wedge in Mixed-Phase Conditions," *SAE 2015 International Conference on Icing of Aircraft, Engines, and Structures*, SAE Paper 2015-01-2116, Jun. 2015. https://doi.org/10.4271/2015-01-2116.

[17] Currie, T., Struk, P., Tsao, J.-C., Fuleki, D., and Knezevici, D., "Fundamental study of mixed-phase icing with application to ice crystal accretion in aircraft jet engines," *4th AIAA Atmospheric and Space Environments Conference*, AIAA Paper 2012-3035, Jun. 2012, p. 3035. https://doi.org/10.2514/6.2012-3035.

[18] Bucknell, A., McGilvray, M., Gillespie, D. R. H., Jones, G., Reed, A., and Collier, B., "Experimental Studies of Ice Crystal Accretion on Axisymmetric Bodies at Aeroengine Conditions," *Journal of Propulsion and Power*, Vol. 36, No. 6, 2020, pp. 836–850. https://doi.org/10.2514/1.B37635.

[19] Knezevici, D., Fuleki, D., Currie, T., and MacLeod, J., "Particle size effects on ice crystal accretion," *4th AIAA Atmospheric and Space Environments Conference*, AIAA Paper 2012-3039, Sep. 2012, p. 3039. https://doi.org/10.2514/6.2012-3039.

[20] Renksizbulut, M., and Yuen, M. C., "Experimental Study of Droplet Evaporation in a High-Temperature Air Stream," *Journal of Heat Transfer*, Vol. 105, No. 2, 1983, pp. 384–388. https://doi.org/10.1115/1.3245590.

[21] Wilhelm, L. R., "Numerical calculation of psychrometric properties in SI units," *Transactions of the ASAE*, Vol. 19, No. 2, 1976, pp. 318–0321. https://doi.org/10.13031/2013.36019.

[22] Kuehn, T. H., and LeRoy, J. T., *Chapter 6: Psychrometrics*, ASHRAE Handbook: Fundamentals, ASHRAE, Atlanta, 2002, pp. 6.1–6.17.

[23] AL-ISMAILI, A. M., and Al-AZRI, N. A., "Simple iterative approach to calculate wet-bulb temperature for estimating evaporative cooling efficiency," *International Journal of Agriculture Innovations and Research*, Vol. 12, No. 6, 2016, p. 13.

[24] Hölzer, A., and Sommerfeld, M., "New simple correlation formula for the drag coefficient of non-spherical particles," *Powder Technology*, Vol. 184, No. 3, 2008, pp. 361 – 365. https://doi.org/10.1016/j.powtec.2007.08.021.

[25] Ouchene, R., Khalij, M., Arcen, B., and Tanière, A., "A new set of correlations of drag, lift and torque coefficients for non-spherical particles and large Reynolds numbers," *Powder Technology*, Vol. 303, 2016, pp. 33 – 43. https://doi.org/10.1016/j.powtec.2016.07.067.

[26] Zastawny, M., Mallouppas, G., Zhao, F., and van Wachem, B., "Derivation of drag and lift force and torque coefficients for non-spherical particles in flows," *International Journal of Multiphase Flow*, Vol. 39, 2012, pp. 227 – 239. https://doi.org/10.1016/j.ijmultiphaseflow.2011.09.004.

[27] Struk, P. M., Ratvasky, T. P., Bencic, T., Zante, J. F. V., King, M. C., Tsao, J.-C., and Bartkus, T. P., "An Initial Study of the Fundamentals of Ice Crystal Icing Physics in the NASA Propulsion Systems Laboratory," *9th AIAA Atmospheric and Space Environments Conference*, AIAA Paper 2017-4242, Jun. 2017. https://doi.org/10.2514/6.2017-4242.

[28] Baumert, A., Bansmer, S., Trontin, P., and Villedieu, P., "Experimental and numerical investigations on aircraft icing at mixed phase conditions," *International Journal of Heat and Mass Transfer*, Vol. 123, 2018, pp. 957–978. https://doi.org/10.1016/j.ijheatmasstransfer.2018.02.008.

[29] Jiji, L. M., *CHAPTER 4: TRANSIENT CONDUCTION*, Heat Conduction, Springer-Verlag Berlin Heidelberg, Berlin, 2009, p. 120.

[30] Fuleki, D., Chalmers, J. L., and Galeote, B., "Technique for Ice Crystal Particle Size Measurements and Results for the National Research Council of Canada Altitude Ice Crystal Test System," *SAE 2015 International Conference on Icing of Aircraft, Engines, and Structures*, SAE Paper 2015-01-2125, Jun. 2015. https://doi.org/10.4271/2015-01-2125.